DØnote 5174-CONF

B_s Mixing in $B_s^0 \to D_s^- e^+ \nu_e X, D_s^- \to \phi\pi^-$ decay mode

The DØ Collaboration
URL *http://www-d0.fnal.gov*

(Dated: July 21, 2006)

A search for $B_s^0 - \overline{B_s^0}$ oscillations was performed using a sample of $B_s^0 \to D_s^- e^+ \nu X$ decays corresponding to approximately 1 fb^{-1} of integrated luminosity accumulated with the DØ Detector in Run II at the Fermilab Tevatron. The flavor of the final state of the B_s meson was determined using the electron charge from the partially reconstructed decay B_s^0, $D_s^- \to \phi\pi^-$, $\phi \to K^+K^-$. An opposite-side tagging method was used for the initial-state flavor determination and using an unbinned log likelihood fit method we obtain a 95% confidence level limit on the oscillation frequency of $\Delta m_s > 7.8$ ps^{-1} and an expected limit of $\Delta m_s = 8.2$ ps^{-1}.

Preliminary Results for Summer 2006 Conferences

I. INTRODUCTION

We report on a first look at reconstruction of $B_s^0 \to D_s^- e^+ \nu_e$ decays, with D_s^- decaying into $\phi\pi^-$ and ϕ decaying to K^+K^-, and a study of B_s oscillations using this decay mode. Although we do not have a dedicated trigger for this mode, we use an inclusive muon sample, where the muon acts as the tag muon for the opposite-side flavor in this sample. Charge conjugated states are implied throughout the note.

The DØ experiment first reported direct limits on the B_s mixing parameter, Δm_s [1], using the $B_s^0 \to D_s \mu \nu_\mu$ decay mode, and CDF subsequently reported a measurement of this parameter at 3.7 σ[2]. As the Tevatron and DØ continues to take data, we hope to improve our result and increase the significance. The addition of this decay mode is a step in that direction and will add to our sensitivity. Currently, the Tevatron is the only place to make this measurement. The measurement is an important test of the CKM formalism of the standard model, and combining it with a measurement of Δm_d will allow us to reduce the error on V_{td}. The standard model predicts, $\Delta m_s = 18.3^{+6.5}_{-1.5}$ ps^{-1} from global fits to the unitarity triangle if the current experimental limits on Δm_s are included in the fit. If information from B_s^0 oscillations limits are not included, global fits give $\Delta m_s = 20.9^{+4.5}_{-4.2}$ ps^{-1} [3, 4]. The analysis described here uses an event-by-event likelihood method to determine the B_s^0 oscillation frequency.

II. DETECTOR DESCRIPTION

The DØ detector is described in detail elsewhere [5, 6]. The following main elements of the DØ detector are essential for this analysis: :

- The magnetic central-tracking system, which consists of a silicon microstrip tracker (SMT) and a central fiber tracker (CFT), both located within a 2-T superconducting solenoidal magnet;
- The liquid-argon/uranium calorimeter;
- The muon system located beyond the calorimeter.

The SMT has 800,000 individual strips, with typical pitch of $50 - 80$ μm, and a design optimized for tracking and vertexing capability at $|\eta| < 3$, where $\eta = -\ln(\tan(\theta/2))$ and θ is the polar angle. The pseudorapidity, $\eta = -\ln\ [\tan(\theta/2)]$ approximates the true rapidity $y = \frac{1}{2}\ \ln[(E + p_z)/(E - p_z)]$, for finite angles in the limit that $(m/E) \to 0$.

The CFT has eight thin coaxial barrels, each supporting two doublets of overlapping scintillating fibers of 0.835 mm diameter, one doublet being parallel to the collision axis, and the other alternating by $\pm 3^\circ$ relative to the axis. The resolution of the impact parameter with respect to the collision point is about 20 μm for 5 GeV tracks.

The three components of the liquid-argon/uranium calorimeter are housed in separate cryostats. A central section, lying outside the tracking system, covers up to $|\eta| = 1.1$. Two end calorimeters extend the coverage to $|\eta| \approx 4$.

The muon system consists of a layer of tracking detectors and scintillation trigger counters inside a 1.8 T iron toroid, followed by two additional layers outside the toroid. Tracking at $|\eta| < 1$ relies on 10 cm wide drift tubes, while 1-cm mini-drift tubes are used at $1 < |\eta| < 2$.

III. DATA SAMPLE

This measurement uses an inclusive muon sample corresponding to approximately 1 fb^{-1} of integrated luminosity, accumulated by DØ during the period from April 2002 to January 2006. B_s^0 hadrons were selected using their semileptonic decays, $B_s^0 \to e^+ \nu D_s^- X$, where $D_s^- \to \phi\pi^-$, $\phi \to K^+K^-$. Charge conjugated states are implied throughout this paper.

For this analysis, the electrons were required to have $p_T > 2$ GeV, to have at least one hit each in the CFT and SMT, to be in the central region $(|\ \eta\ |) < 1.1$, to have energy deposit in the electromagnetic calorimeter consistent with an electron $0.55 < E/p < 1.02$ and low energy deposit in the hadron calorimeter with electromagnetic fraction greater than 0.7. The cuts are chosen to select electrons with about 90% purity [7]. We also require that there is no muon in a cone of 0.7 around the electron. i.e. $(\Delta R_{e,\mu} = \sqrt{{\Delta\phi_{e,\mu}}^2 + {\Delta\eta_{e,\mu}}^2} > 0.7)$, where $\Delta\phi_{e,\mu}$ is the ϕ difference between electron and muon and $\Delta\eta_{e,\mu}$ is the difference in η between electron and muon.

---

[1] We use $\hbar = 1$, c=1 convention throughout the note

The primary vertex position in the transverse plane was determined on an event-by-event basis by requiring the tracks in the event to come from a common collision point that is constrained by the mean beam-spot position calculated on a run-by-run basis. The tracks used in the reconstruction of the B_s^0 semileptonic decay were excluded from the primary vertex fit.

All charged particles in the event were clustered into jets using the DURHAM clustering algorithm [8] with a p_T cut-off parameter set at 15 GeV [9]. The D_s^- candidate was constructed from three tracks included in the same jet as the reconstructed electron. Two oppositely charged tracks were assigned the kaon mass and were required to form a ϕ meson satisfying $1.004 < M(K^+K^-) < 1.034$ GeV. The third track was assigned the pion mass and was required to have a charge opposite to that of the electron. All three tracks were required to have at least one hit in both the SMT and CFT. The transverse momentum requirements were $p_T > 0.7$ GeV for the kaons and $p_T > 0.5$ GeV for the pion. The three tracks were required to form a common D_s^- vertex with $\chi^2_D < 16$ for the vertex fit. The vertexing algorithm is described in detail in Ref. [10]. For each particle, the transverse ϵ_T and longitudinal ϵ_L projections of the track impact parameter with respect to the primary vertex, together with the corresponding uncertainties $\sigma(\epsilon_T)$ and $\sigma(\epsilon_L)$, were computed. The combined significance $\sqrt{(\epsilon_T/\sigma(\epsilon_T))^2 + (\epsilon_L/\sigma(\epsilon_L))^2}$ was required to be greater than 4 for the kaons. The distance d_T^D between the primary and D_s^- vertices in the transverse plane was required to exceed 4 standard deviations, that is, $d_T^D/\sigma(d_T^D) > 4$. The angle α_T^D between the D_s^- momentum and the direction from the primary vertex to the D_s^- vertex in the transverse plane was required to satisfy the condition $\cos(\alpha_T^D) > 0.9$.

The tracks of the electron and D_s^- candidate were required to produce a common B_s^0 vertex with $\chi^2_B < 9$ for the vertex fit. The transverse momentum of the B_s^0 candidate, $p_T^{e^+D_s^-}$, was defined as the vector sum of the transverse momenta of the electron and the D_s^- candidate. The mass of the $(e^+D_s^-)$ system was required to be within the range $2.6 < M(e^+D_s^-) < 5.4$ GeV. The transverse decay length of the B_s^0 hadron, d_T^B, was defined as the distance in the transverse plane between the primary vertex and the vertex produced by the electron and the D_s^- meson. If the distance d_T^B exceeded $4 \cdot \sigma(d_T^B)$, the angle α_T^B between the B_s^0 momentum and the direction from the primary to the B_s^0 vertex in the transverse plane was required to satisfy the condition $\cos(\alpha_T^B) > 0.95$. The distance d_T^B was allowed to be greater than d_T^D, provided that the distance between the B_s^0 and D_s^- vertices, d_T^{BD}, was less than $2 \cdot \sigma(d_T^{BD})$.

The final event samples were selected using a Likelihood Ratio Method, described below.

A. Likelihood Ratio Method

In the Likelihood Ratio Method, a set of discriminating variables, $x_1, ...x_n$, is constructed for a given event. The probability density functions (*pdf*s), $f_i^s(x_i)$ for the signal and $f_i^b(x_i)$ for the background, are built for each variable x_i. The combined selection variable y is defined as

$$y = \prod_{i=1}^{n} y_i; \quad y_i = \frac{f_i^b(x_i)}{f_i^s(x_i)}. \tag{1}$$

The variable x_i can be undefined for some events. In this case, the corresponding variable y_i is set to unity. The selection of the signal is obtained by applying a cut $y < y_0$ [11]. For uncorrelated variables $x_1, ...x_n$, the selection using the combined variable y gives the best possible performance, i.e., the maximal signal efficiency for a given background efficiency.

The following discriminating variables were used:

- Helicity angle, defined as the angle between the D_s^- and K^+ momenta in the (K^+K^-) center-of-mass system. (The K^+ and K^- mesons decay back-to-back in the ϕ rest frame so the choice of K^+ over K^- is arbitrary);
- Isolation, computed as $Iso = p^{tot}(e^+D_s^-)/(p^{tot}(e^+D_s^-) + \sum p_i^{tot})$. The sum $\sum p_i^{tot}$ is taken over all charged particles in the cone $\sqrt{(\Delta\phi)^2 + (\Delta\eta)^2} < 0.5$, where $\Delta\eta$ and $\Delta\phi$ are the pseudorapidity and the azimuthal angle with respect to the $(e^+D_s^-)$ direction. The e^+, K^+, K^- and π^- momenta are not included in the sum;
- $p_T(K^+K^-)$;
- Invariant mass, $M(e^+D_s^-)$;
- χ^2 of the D_s^- vertex fit;
- Invariant mass, $M(K^+K^-)$.

The probability density functions were constructed using the real data events. For each channel, three bands, B_1, B_2 and S, were defined as:

$$\begin{aligned} B_1 &: 1.75 < M(D_s^-) < 1.79 \text{ GeV}; \\ B_2 &: 2.13 < M(D_s^-) < 2.17 \text{ GeV}; \\ S &: 1.92 < M(D_s^-) < 2.00 \text{ GeV}. \end{aligned}$$

The background probability density function for each variable was constructed using events from the B_1 and B_2 bands. The signal probability density function was constructed by subtracting the background, obtained as a sum of the distributions in the B_1 and B_2 bands, from the distribution of events in band S.

The final cut on the combined variable, $-\log_{10} y > 0.12$, was selected by requiring the maximal value of $N_S/\sqrt{N_S + N_{B_1} + N_{B_2}}$, where N_S, N_{B_1} and N_{B_2} are the number of events in bands S, B_1 and B_2, respectively.

B. Mass Fitting Procedure

To fit the $M_{KK\pi}$ distribution of the selected candidates (Fig. 1), we use single Gaussians g_1 and g_2 to describe the $D_s^{\pm} \to \phi\pi$ and $D^{\pm} \to \phi\pi$ decay respectively, and the background is modeled by a second degree polynomial f_{bkg} (see Fig. 1). The fitting function is given in Eqn. 2.

$$\begin{aligned} g_1 &= \frac{(p0 * bw)}{\sqrt{(2\pi)}p2} e^{-\frac{1}{2}(\frac{(x-p1)}{p2})^2} \\ g_2 &= \frac{(p3 * bw)}{\sqrt{(2\pi)}p5} e^{-\frac{1}{2}(\frac{(x-p4)}{p5})^2} \\ f_{bkg} &= p6 + p7 * x + p8 * x^2 \end{aligned} \tag{2}$$

where bw is the binwidth. The fit parameters p0 and p3, therefore directly give the number of events in the peak. x is the D_s mass. We obtain 1012 ± 63 D_s signal candidates, and 284 ± 60 $D^{\pm}$ candidates.

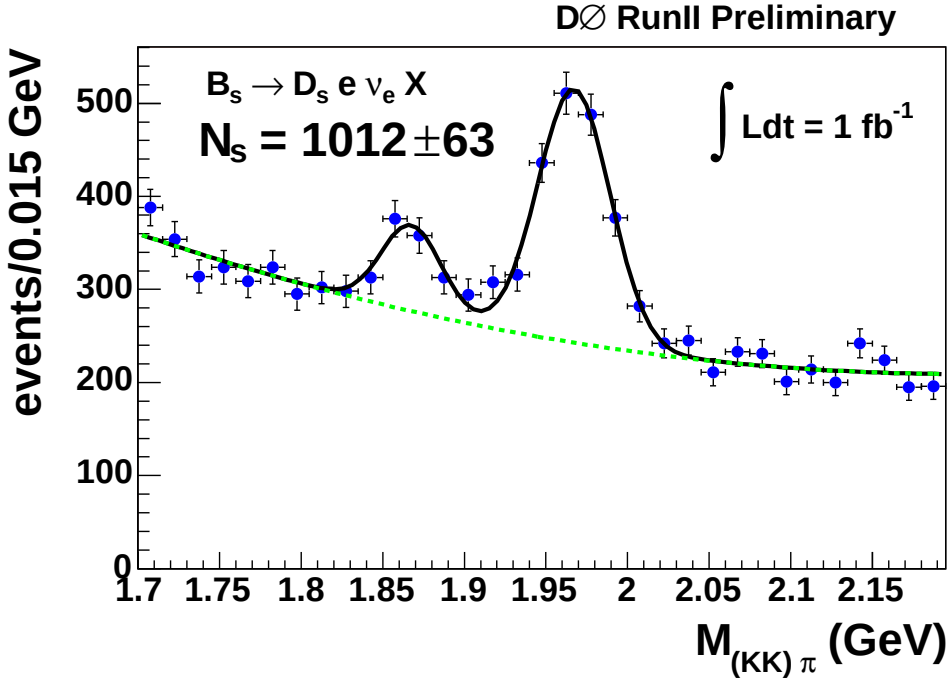

FIG. 1: All tagged B_s candidates. The flavor tagging is discussed in the next section Sec. IV

Muon Tag	988 ± 52
SVCharge Tag	11 ± 5
Electron Tag	5 ± 3
Combined Tag	1012 ± 63

TABLE I: Number of tagged events

IV. INITIAL STATE FLAVOR TAGGING

A necessary step in the B_s^0 oscillation analysis is the determination of the $B_s^0/\bar{B_s^0}$ initial- and final-state flavors. The presence of the electron in the B_s^0 semileptonic decay allows a determination of the final-state flavor since the b-quark flavor is correlated with the charge of the electron in the decays $B_s^0 \to e^+ X$ and $\bar{B_s^0} \to e^- X$.

The flavor of the initial state of the signal B_s^0 was determined using a likelihood ratio method (see Sec. III A), based on the properties of the other b-hadron in the event (opposite side tagging). We define variables which distinguish between a b and a $\bar{b}$ quark. The pdf's for the combined tagging variable y (see Equation 1) were determined from $B^+ \to \mu^+ \nu\ \bar{D}^0$data events in which the final state B flavor is given by the sign of the muon.

For events with a reconstructed muon on the opposite side of the B ($\cos\phi(\mathbf{p}_\mu, \mathbf{p}_B) < 0.8$), a muon jet charge was defined as a discriminating variable. The muon jet charge was defined as: $Q_J^\mu = \sum_i \frac{q^i p_T^i}{p_T^i}$, where the sum was taken over all charged particles on the opposite side, including the muon, which were within a cone of $\Delta R = \sqrt{(\Delta\phi)^2 + (\Delta\eta)^2} < 0.5$ around the muon direction.

For events without an identified muon but with a reconstructed electron on the opposite side, the electron jet charge $Q_J^e = \sum_i \frac{q^i p_T^i}{p_T^i}$, defined similarly to the muon jet charge, was used.

For events with no muon or electron, an event charge was used as a discriminating variable: $Q_{EV} = \sum_i \frac{q^i p_T^i}{p_T^i}$, where the sum was taken over all charged particles with $0.5 < p_T < 50$ GeV and having $\cos\phi(\mathbf{p}, \mathbf{p}_B) < 0.8$.

Finally, in any event with a reconstructed secondary vertex, the secondary vertex charge was also used as a discriminating variable. The secondary vertex charge was defined as: $Q_{SV} = \sum_i \frac{(q^i p_L^i)^{0.6}}{(p_L^i)^{0.6}}$, where the sum was taken over all particles included in the secondary vertex, and p_L^i is the longitudinal momentum of a given particle with respect to the sum of all the momenta of the particles associated with the secondary vertex.

The discriminating variables are combined to construct the tag variable d defined in Sec. III A. In the context of flavor tagging we called it the "predicted dilution", defined below:

$$d_{pr} = \frac{1-y}{1+y}. \tag{3}$$

The variable d_{pr} changes between -1 and 1. An event with $d_{pr} > 0$ is tagged as b quark and that with $d_{pr} < 0$ as a $\bar{b}$ quark, with larger $|d_{pr}|$ values corresponding to higher tagging purities.

An important property of opposite side tagging is the independence of its performance on the type of the reconstructed B meson, since the hadronization of the two b quarks is not correlated in $p\bar{p}$ interactions. Therefore, the flavor tagging algorithm can be calibrated in data by applying it to the events with the B^0 and B^+ decays. The measured performance can then be used in the study of B_s^0 meson oscillations. This tagging method was tested and calibrated extensively on both Monte Carlo and real data $B \to \mu^+ \nu D^{*-}$ events [12]. From fits to the asymmetry distribution, one extracted the B_d oscillation parameter Δm_d, with value consistent with the world average value [13].

In our sample, since we always have a trigger muon in the event, we expect the sample to be mostly muon tagged and this is what we find. 98% of the tagged events come from a muon tag. We look for a muon tag first, then an SVCharge and electron tag. From a fit to D_s invariant mass for each individual tagger, the number of tagged events obtained are given in table I.

The mass distributions for the tagged samples tagged by the individual taggers are shown in Figs. 2-4.

For more details on the initial state flavor tagging technique, see Ref. [12].

V. EXPERIMENTAL OBSERVABLES

The proper lifetime of the B_s^0 meson, $c\tau_{B_s^0}$, for semileptonic decays can be written as

$$c\tau_{B_s^0} = x^M \cdot K, \quad \text{where} \quad x^M = \left[\frac{\mathbf{d_T^B} \cdot \mathbf{p_T^{eD_s^-}}}{(p_T^{eD_s^-})^2} \right] \cdot cM_B. \tag{4}$$

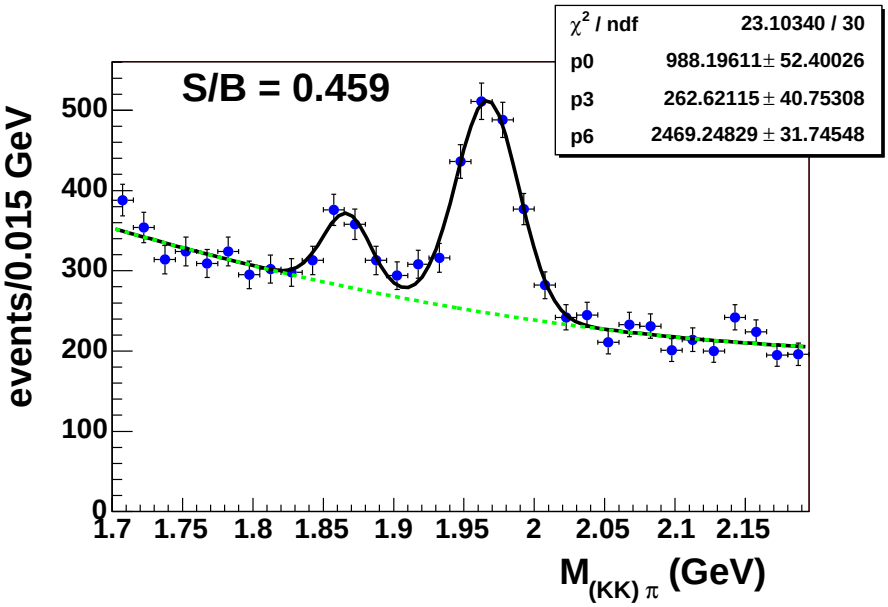

FIG. 2: Selected B_s candidates requiring the muon tag

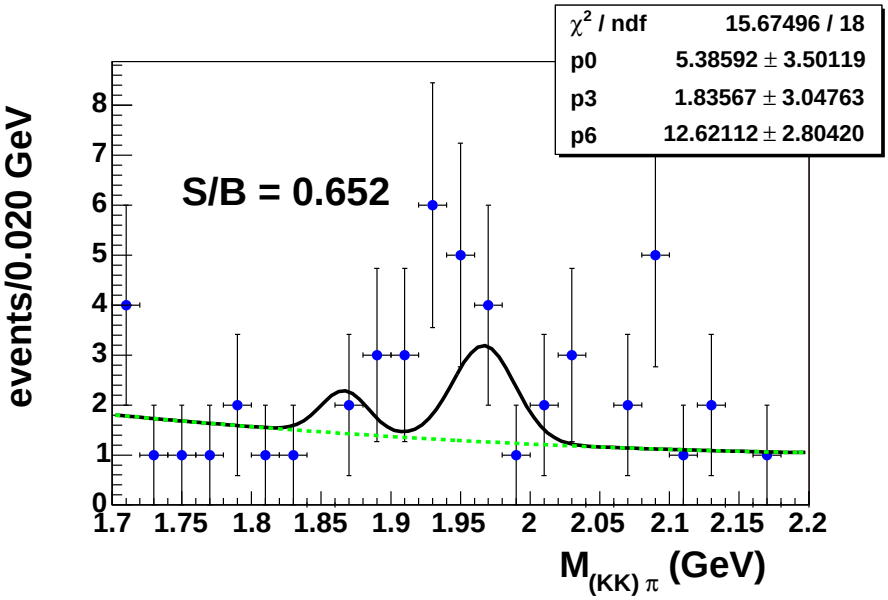

FIG. 3: Selected B_s candidates which have an electron tag

x^M is the *visible proper decay length*, or VPDL, and K is the correction factor, also called the K factor. Semileptonic B decays necessarily have an undetected neutrino present in the decay chain, making a precise determination of the kinematics for the B meson impossible. In addition, other neutral or non-reconstructed charged particles can be present in the decay chain of the B meson. This leads to a bias towards smaller values of the B momentum, which is calculated using the reconstructed particles. A common practice to correct this bias is to scale the measured momentum of the B candidate by a K factor, which takes into account the effects of the neutrino and other lost or non-reconstructed particles. For this analysis, the K factor was defined as

$$K = p_T(e^+ D_s^-)/p_T(B_s^0), \tag{5}$$

where p_T denotes the absolute value of the transverse momentum. The K-factor distributions used to correct the data were obtained from the Monte Carlo (MC) simulation.

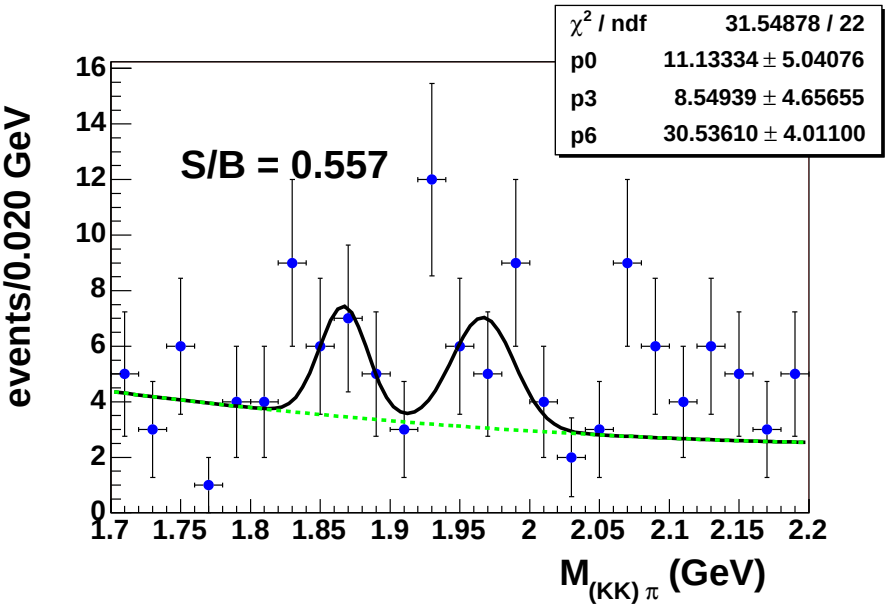

FIG. 4: Selected B_s candidates which have a SVCharge tag

VI. FITTING PROCEDURE

All tagged events with $1.72 < M(K^+K^-\pi^-) < 2.22$ GeV were used in the unbinned likelihood fitting procedure. The likelihood for an event to arise from a specific source in the sample depends on the x^M, its uncertainty (σ_{x^M}), the mass of the D_s^- meson candidate (m), the predicted dilution (d_{pr}) and the selection variable y described in Section III A. All of the quantities used in the unbinned likelihood fitting procedure are known on an event-by-event basis. The *pdf* for each source can be expressed by the product of the corresponding *pdf*s:

$$f_i = P_i^{x^M}(x^M, \sigma_{x^M}, d_{pr}) P_i^{\sigma_{x^M}} P_i^m P_i^{d_{pr}} P_i^y. \tag{6}$$

The VPDL *pdf* $P_i^{x^M}(x^M, \sigma_{x^M}, d_{pr})$ represents a conditional probability, therefore it should be multiplied by $P_i^{\sigma_{x^M}}$ and $P_i^{d_{pr}}$ to have a joint *pdf* (see "Probability" section in PDG [13]). The *pdf*s P_i^m and P_i^y are used for separation of signal and background.

The following sources, i, were considered:

- $e^+D_s^-(\to \phi\pi^-)$ signal with fraction $\mathcal{F}_{eD_s}$.
- $e^+D^-(\to \phi\pi^-)$ signal with fraction $\mathcal{F}_{eD^\pm}$.
- Combinatorial background with fraction $(1 - \mathcal{F}_{eD_s} - \mathcal{F}_{eD^\pm})$.

The fractions $\mathcal{F}_{eD_s}$ and $\mathcal{F}_{eD^\pm}$ were determined from the mass fit (see Fig. 1). The total probability density function for a B candidate has the form

$$F_n = \mathcal{F}_{eD_s} f_{eD_s} + \mathcal{F}_{eD^\pm} f_{eD^\pm} + (1 - \mathcal{F}_{eD_s} - \mathcal{F}_{eD^\pm})\, f_{bkg}. \tag{7}$$

The following form was minimized using the MINUIT [14] program:

$$\mathcal{L} = -2 \sum_n \ln F_n, \tag{8}$$

where n varies from 1 to $N_{total\ tagged\ events}$.

The *pdf*s for the VPDL uncertainty ($P_i^{\sigma_{x^M}}$) (Fig. 5), mass (P_i^m)(Fig. 1), dilution ($P_i^{d_{pr}}$)(Fig. 6), and selection variable y (P_i^y)(Fig. 7) were taken from experimental data. The signal *pdf*s were also used for the $e^+D^-(\to \phi\pi^-)$ signal. We describe how we obtain them in the following sections.

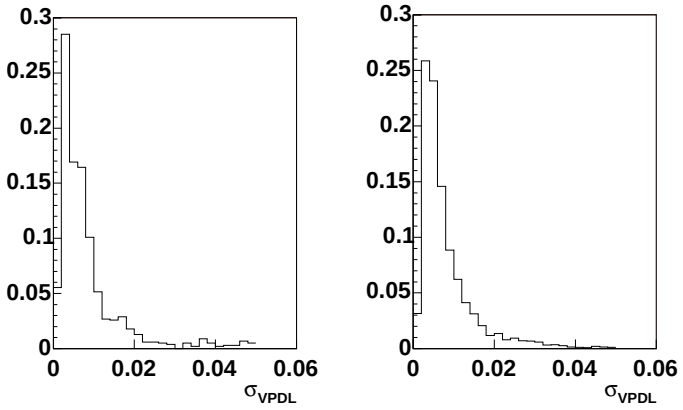

FIG. 5: Distributions of VPDL errors for signal and combinatorial background.

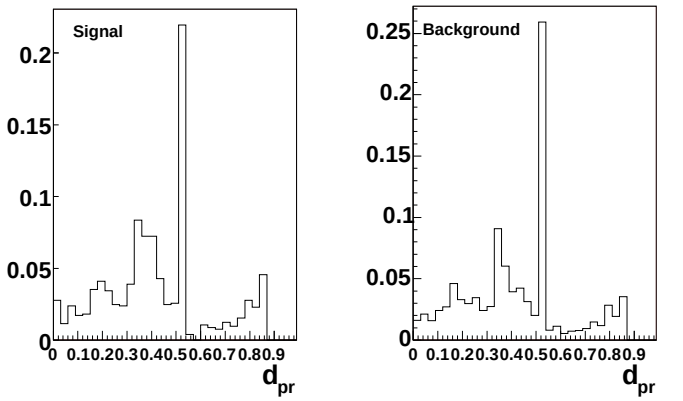

FIG. 6: Distributions of predicted dilution for signal and combinatorial background.

A. PDF for eD_s Signal

The eD_s sample is composed mostly of B_s^0 mesons with some contributions from B_u and B_d mesons. Different species of B mesons behave differently with respect to oscillations. Neutral B_d and B_s mesons do oscillate (with different frequencies) while charged B_u mesons do not. The possible contributions of b-baryons in the sample are expected to be small and so are neglected.

For a given type of B-hadron (i.e. d, u, s), the distribution of the visible proper decay length x is given by:

$$p_s^{nos}(x, K, d_{pr}) = \frac{K}{c\tau_{B_s}} \exp(-\frac{Kx}{c\tau_{B_s}}) \cdot 0.5 \cdot (1 + \mathcal{D}(d_{pr}) \cos(\Delta m_s \cdot Kx/c)) \tag{9}$$

$$p_s^{osc}(x, K, d_{pr}) = \frac{K}{c\tau_{B_s}} \exp(-\frac{Kx}{c\tau_{B_s}}) \cdot 0.5 \cdot (1 - \mathcal{D}(d_{pr}) \cos(\Delta m_s \cdot Kx/c)) \tag{10}$$

$$p_{DsDs}^{osc}(x, K) = \frac{K}{c\tau_{B_s}} \exp(-\frac{Kx}{c\tau_{B_s}}) \cdot 0.5 \tag{11}$$

$$p_{DsDs}^{nos}(x, K) = \frac{K}{c\tau_{B_s}} \exp(-\frac{Kx}{c\tau_{B_s}}) \cdot 0.5 \tag{12}$$

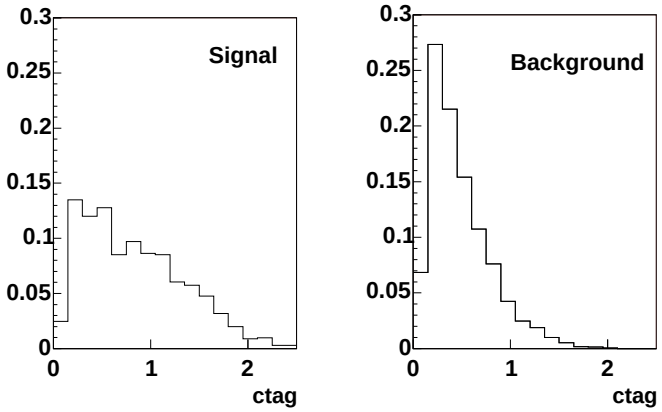

FIG. 7: Signal selection function for signal and combinatorial background.

$$p_u^{nos}(x,K,d_{pr}) = \frac{K}{c\tau_{B_u}} \exp(-\frac{Kx}{c\tau_{B_u}}) \cdot 0.5 \cdot (1 - \mathcal{D}(d_{pr})) \tag{13}$$

$$p_u^{osc}(x,K,d_{pr}) = \frac{K}{c\tau_{B_u}} \exp(-\frac{Kx}{c\tau_{B_u}}) \cdot 0.5 \cdot (1 + \mathcal{D}(d_{pr})) \tag{14}$$

$$p_d^{nos}(x,K,d_{pr}) = \frac{K}{c\tau_{B_d}} \exp(-\frac{Kx}{c\tau_{B_d}}) \cdot 0.5 \cdot (1 - \mathcal{D}(d_{pr}) \cos(\Delta m_d \cdot Kx/c)) \tag{15}$$

$$p_d^{osc}(x,K,d_{pr}) = \frac{K}{c\tau_{B_d}} \exp(-\frac{Kx}{c\tau_{B_d}}) \cdot 0.5 \cdot (1 + \mathcal{D}(d_{pr}) \cos(\Delta m_d \cdot Kx/c)) \tag{16}$$

where, τ_{B_s} is the lifetime of the B-hadron. Note that there is a sign swap in Eq. 13–16 with respect to 9 and 10 due to anti-correlation of charge for electrons from $B \to DD_s$; $D \to eX$ processes.

K is the K-factor given by eqn. 17, which reflects the difference between the observable and true momenta of the B-hadron. The K-factors are obtained from simulated events, where we require the event to pass reconstruction cuts and be matched to a B meson, using truth information. $P_T^{eD_s^-}$ is the reconstructed P_T sum of the e and D_s^- candidate, and P_T^B is the generator level P_T of the matched B meson.

$$\text{where } \; K = P_T^{eD_s^-}/P_T^B, \tag{17}$$

The dilution calibration is given by the following equation (Ref. [12] and Ref. [1]):

$$\begin{aligned} \mathcal{D}(d_{pr})\,\big|_{d_{pr}<0.6} &= 0.457 \cdot |d_{pr}| + 2.349 \cdot |d_{pr}|^2 - 2.498 \cdot |d_{pr}|^3, \\ \mathcal{D}(d_{pr})\,\big|_{d_{pr}>0.6} &= 0.6. \end{aligned} \tag{18}$$

The translation to the measured VPDL, x^M is achieved by a convolution of the K-factors and resolution functions as specified below.

$$P^{osc,\ nos}_{(d,u,s),\ j}(x^M,\sigma_{x^M},d_{pr}) = \int_{K_{min}}^{K_{max}} dK\ D_j(K) \cdot \frac{Eff_j(x^M)}{N_j(K,\sigma_{x^M},d_{pr})} \int_0^\infty dx\ G(x-x^M,sf,\sigma_{x^M}) \cdot p^{osc,\ nos}_{(d,u,s),\ j}(x,K,d_{pr}), \tag{19}$$

$$\text{Here } G(x-x^M,sf,\sigma_{x^M}) = \frac{1}{\sqrt{2\pi}\sigma_{x^M}} \exp\left(-\frac{(x-x^M)^2}{2\ (sf*\sigma_{x^M})^2}\right) \tag{20}$$

$Eff_j(x)$ is the reconstruction efficiency as a function of VPDL, for a given decay channel j of u,d, or s type of B meson. This includes the decay mode $B_s \to D_s D_s$ given by equations, 11 and 12. More details on the decay modes which contribute to the candidates, is given in Sec. VII.

The detector resolution on VPDL is σ_{x^M}. We introduce a resolution scale factor, sf, to the VPDL resolution, which we obtain from an independant sample for the signal, as discussed in Sec. VII, and for the background, it is estimated from the lifetime fit of the background region, discussed in Sec. VII. The function $D_j(K)$ gives the normalized distribution of the K-factor in a given channel j. We use K-factor histograms, so instead of an integration, we sum over the K-factor bins. The K-factor's for the signal can be seen in Fig. 10 and the same but binned in $m_{D_s^- e}$ can be seen in figures Fig. 11 and Fig. 12.

The normalization factor N_j is calculated by integration over the entire VPDL region:

$$N_j(K, \sigma_{x^M}, d_{pr}) = \int_{-\infty}^{\infty} dx^M \; Eff_j(x^M) \int_0^{\infty} dx \; G(x - x^M, sf, \sigma_{x^M}) \cdot \left(p^{osc}_{(d,u,s),\ j}(x, K, d_{pr}) + p^{nos}_{(d,u,s),\ j}(x, K, d_{pr}) \right) \tag{21}$$

The total VPDL PDF for the eD_s signal is a sum of all the contributions which give the D_s mass peak:

$$P^{osc,\ nos}_{eD_s}(x^M, \sigma_{x^M}, d_{pr}) = \left(\sum_j F_j \cdot P^{osc,\ nos}_{d,\ j}(x^M, \sigma_{x^M}, d_{pr}) + \sum_j F_j \cdot P^{osc,\ nos}_{u,\ j}(x^M, \sigma_{x^M}, d_{pr}) + \sum_j F_j \cdot P^{osc,\ nos}_{s,\ j}(x^M, \sigma_{x^M}, d_{pr}) \right) \cdot (1 - fr_{c\bar{c}}) + fr_{c\bar{c}} \cdot P^{osc,\ nos}_{c\bar{c}}(x^M) \tag{22}$$

Here the sum $\sum_j$ is taken over all decay channels $B \to e^+ \nu D_s^- X$ and F_j is the fraction of a given channel j contributing to the signal, which includes the acceptance, reconstruction efficiencies and branching fractions. The evaluation of the sample composition is given in Sec. VII. $P^{osc,\ nos}_{c\bar{c}}(x^M)$ is given by a double gaussian function which is fitted to the VPDL distribution of $c\bar{c}$ events. We use simulated $c\bar{c}$ events, where one of the charm mesons decays into an electron, and which satisfy all the reconstruction cuts for the signal selection. The VPDL for the $c\bar{c}$ contribution can be seen in Fig. 8. The resolutions obtained for the first and second gaussians are 70 ± 3 μm and 425 ± 30 μm, with a 20% contribution from the wider gaussian.

The functions $D_j(K)$ were taken from the MC simulation. Uncertainties in all these inputs will contribute to the systematic uncertainties.

The B meson lifetimes and efficiencies $Eff_j(x)$ are highly correlated. The efficiencies determined using MC do not take into account the trigger selection and therefore measurements of the B meson lifetimes with such efficiencies give biased results. The lifetime does not influence directly the measurements of the B_s^0 oscillation frequency. However, its modelling does affect the error. Therefore the B_s^0 lifetime was determined from data using the efficiencies determined from the MC.

B. *pdf* for Combinatorial Background

The following contributions to the combinatorial background were considered:

1. Prompt background, with *pdf* P_{bkg} and with the $e^+ D_s^-$ vertex coinciding with the primary vertex (described as a Gaussian with a width determined by the resolution; fraction in the background: $\mathcal{F}_0$). The resolution scale factor for this background is different from the signal resolution scale factor. The scale factor is a free fit parameter, s_{bkg}.

2. Background (*pdf* P^{res}_{bkg}) with fake vertices (random tracks forming a vertex), distributed around the primary vertex (described as a Gaussian with constant width σ_{peak_bkg}; fraction in the background: $\mathcal{F}_{peak\_bkg}$).

3. Long-lived background, with *pdf* p^{long}_{bkg} (exponential with constant decay length $c\tau_{bkg}$ convoluted with the resolution). This background was divided into three subsamples:

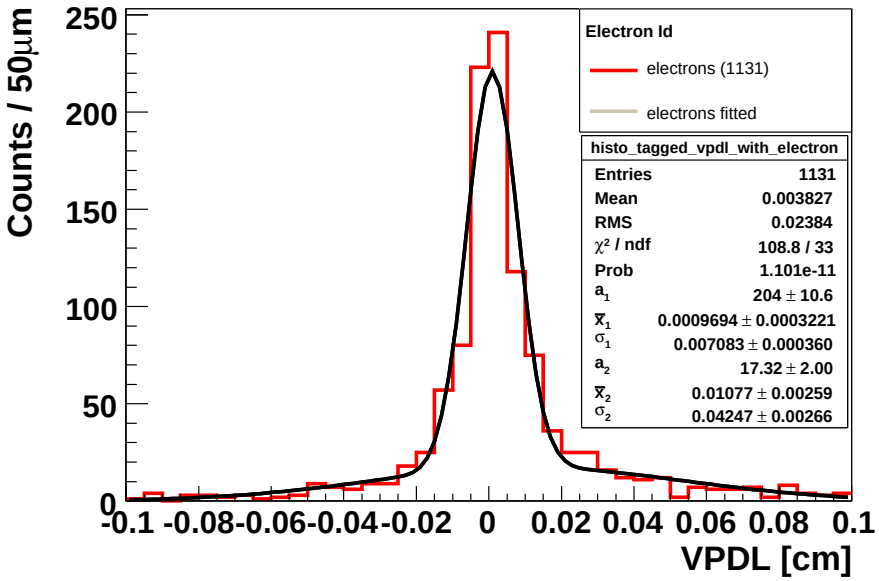

FIG. 8: $c\bar{c}$ VPDL resolution where one of the charm mesons decays into an electron

(a) insensitive to the tagging (fraction in the long-lived background: $(1-\mathcal{F}_{tsens})$);

(b) sensitive to the tagging and non-oscillating (fraction in the background sensitive to the tagging: $(1-\mathcal{F}_{osc})$);

(c) sensitive to the tagging and oscillating with frequency Δm_d (fraction in the background sensitive to the tagging: $\mathcal{F}_{osc}$).

The fractions of these contributions and their parameters were determined from the data sample from the background lifetime fit.

The background *pdf* was expressed in the following form:

$$P_{bkg}(x^M,\sigma_{x^M},d_{pr}) = \mathcal{F}_{peak\_bkg}G(0-x^M,\sigma_{peak\_bkg})+(1-\mathcal{F}_{peak\_bkg})\cdot P^{res}_{bkg}(x^M,\sigma_{x^M}), \quad (23)$$

$$P^{res}_{bkg}(x^M,\sigma_{x^M},d_{pr}) = \frac{Eff(x^M)}{N}\int_0^\infty dx\left(\mathcal{F}_0 G(x-x^M,s_{bkg}\sigma_{x^M})\delta(x)+(1-\mathcal{F}_0)G(x-x^M,\sigma_{x^M})\cdot p^{long}_{bkg}\right),$$

$$p^{long,osc/nos}_{bkg}(x,d_{pr}) = \frac{1}{c\tau_{bkg}}\exp\left(-\frac{x}{c\tau_{bkg}}\right)\times \quad (24)$$
$$\left((1-\mathcal{F}_{tsens})+\mathcal{F}_{tsens}\left((1\pm\mathcal{D})(1-\mathcal{F}_{osc})+(1\pm\mathcal{D}\cos\left(\Delta m_d\cdot x/c\right))\cdot\mathcal{F}_{osc}\right)\right),$$

where N is a normalization constant and the fit parameters are $\mathcal{F}_{peak\_bkg}$, σ_{peak_bkg}, $\mathcal{F}_0$, $\mathcal{F}_{tsens}$, $\mathcal{F}_{osc}$ and $c\tau_{bkg}$. As an efficiency $Eff(x^M)$, the efficiency for the $B^0_d\to D^-\mu^+\nu X$ channel was used.

VII. FIT INPUTS

We have used the following measured parameters for B mesons from the PDG [13] as inputs for the lifetime fitting procedure: $c\tau_{B^+}=501$ μm, $c\tau_{B^0_d}=460$ μm, and $\Delta m_d=0.502$ ps^{-1}. The latest PDG values were also used to determine the branching fractions of decays contributing to the D^-_s sample. We used the event generator EvtGen [15] since this code was developed specifically for the simulation of B decays. For those branching fractions not given in the PDG, we used the values provided by EvtGen, which are motivated by theoretical considerations.

Taking into account the corresponding branching rates and reconstruction efficiencies, we calculated the contributions to our signal region from various processes. The $B^0_s\to D^-_s e^+\nu X$ modes (including through D^{*-}_s, D^{*-}_{s0}, and $D^{'-}_{s1}$ and e^+ originating from τ decays) comprise $89.7\pm3.0\%$ of our sample, including reconstruction efficiency. Other backgrounds with both a real D^-_s and e^+ and showing up in the peak, but not expected to oscillate with Δm_s, that are considered are $B\to D^+_{(s)}D^-_s X$ decays followed by $D^+_{(s)}\to e^+\nu X$. Taking into account the uncertainties in input branching fractions, the sample composition of the decay modes contributing to the signal is given below:

- $B_s^0 \to e^+\nu D_s^-$: $(22.0 \pm 1.0)\%$;
- $B_s^0 \to e^+\nu D_s^{-*} \to e^+\nu D_s^- X$: $(62.8 \pm 2.7)\%$;
- $B_s^0 \to e^+\nu D_{s0}^{*-} \to e^+\nu D_s^- X$: $(1.8 \pm 0.1)\%$;
- $B_s^0 \to e^+\nu D_{s1}^{'-} \to e^+\nu D_s^- X$: $(3.1 \pm 0.1)\%$;
- $B_s^0 \to \tau^+\nu D_s^- \to e^+\nu D_s^- X$: $(1.9 \pm 0.7)\%$;
- $B_s^0 \to D_s^+ D_s^- X; D_s^- \to e\nu X$: $(3.5 \pm 2.6)\%$;
- $B_s^0 \to D D_s^- X; D \to e\nu X$: $(0.8 \pm 0.3)\%$;
- $B^+ \to D D_s^- X; D \to e\nu X$: $(2.02 \pm 0.1)\%$;
- $B^0 \to D D_s^- X; D \to e\nu X$: $(2.05 \pm 0.2)\%$;

We then determined the efficiency of the lifetime selections for the sample as a function of VPDL. Fig. 9 shows the efficiency as a function of lifetime for the decay $B_s^0 \to D_s^- e^+\nu X$.

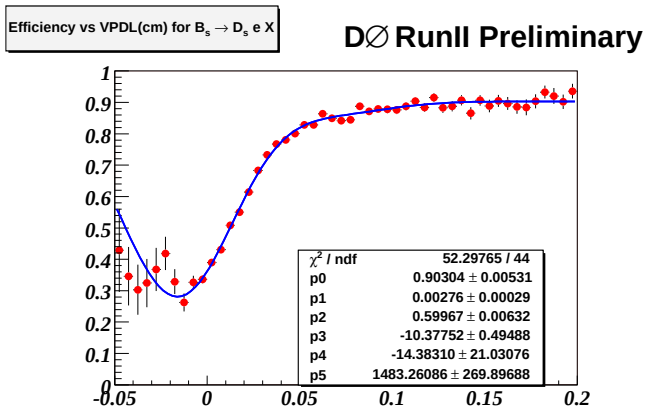

FIG. 9: Efficiency of the lifetime-dependent cuts as a function of VPDL for $B_s^0 \to e^+\nu D_s^- X$.

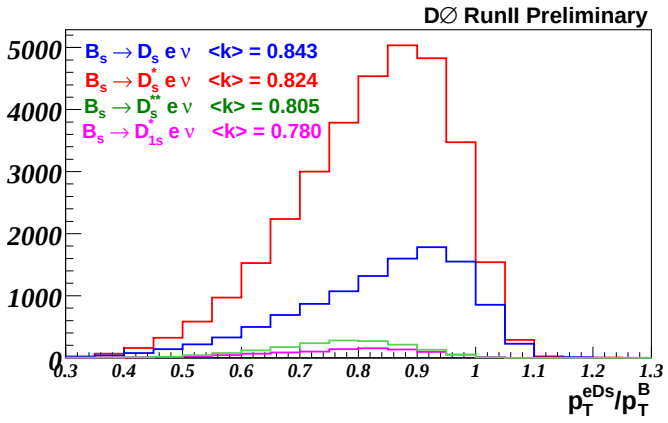

FIG. 10: K factor distributions for $B_s^0 \to e^+\nu D_s^-$; $B_s^0 \to e^+\nu D_s^-$, $B_s^0 \to e^+\nu D_s^{*-} \to e^+\nu D_s^-$, $B_s^0 \to e^+\nu D_s^{**-} \to e^+\nu D_s^-$, and $B_s^0 \to e^+\nu D_{1s}^{*-} \to e^+\nu D_s^-$ processes.

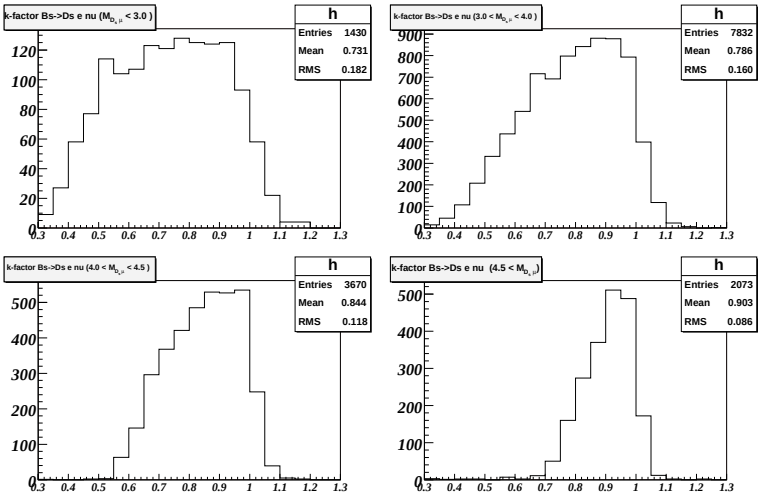

FIG. 11: K factor in bins of mass$(D_s^- e)$ for $B_s^0 \to e^+\nu D_s^-$ decays.

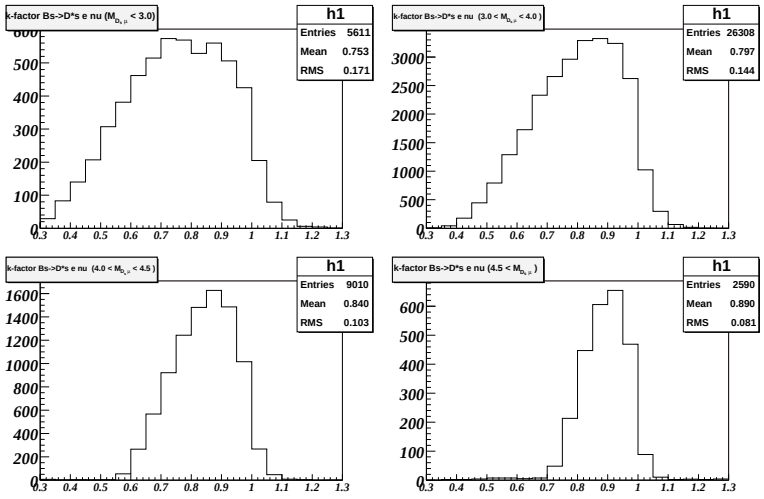

FIG. 12: K factor versus mass($D_s^- e$) for $B_s^0 \to e^+ \nu D_s^{*-} \to e^+ \nu D_s^-$ decays.

In determining the K factor distributions, MC generator-level information was used for the computation of p_T. Following the definition used in Eq. 5, the K factor distributions for all considered decays were determined. Figure 10 shows the distributions of the K factors for the semi-electronic decays of the B_s^0 meson. As expected, the K factors for D_s^{-*}, D_{s0}^{*-} and $D_{s1}^{'-}$ have lower mean values because more decay products are lost. Note that since the K factors in Eq. 5 were defined as the ratio of transverse momenta, they can exceed unity.

The VPDL uncertainty was estimated by the vertex fitting procedure. A resolution scale factor was introduced to take into account a possible bias. It was determined using the $J/\psi \to e^+e^-$ sample. The mass distribution for the J/ψ candidates is shown in Fig. 13.

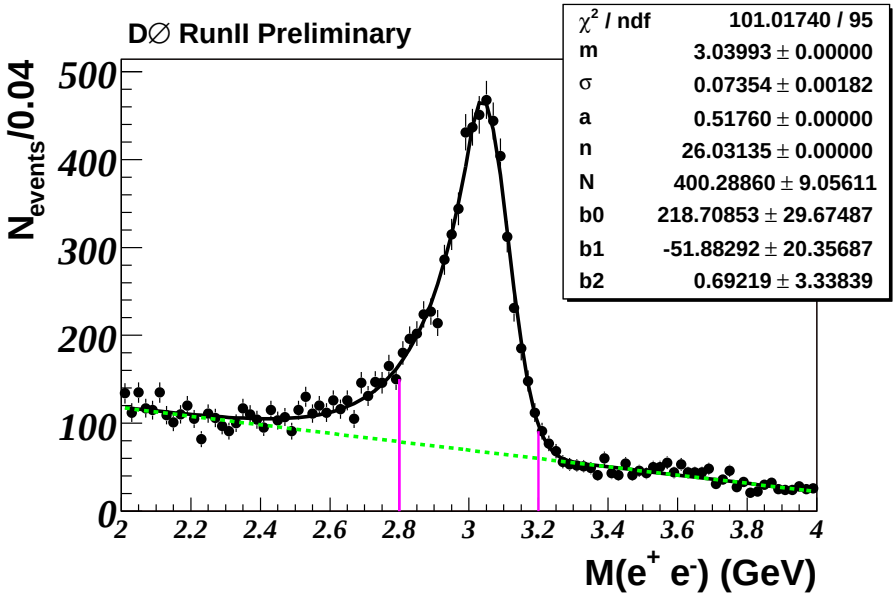

FIG. 13: Mass distribution of $J/\psi \to e^+e^-$ candidates.

Figure 14 shows the pull distribution, $PDL_{J/\psi}/\sigma(PDL_{J/\psi})$, of the J/ψ vertex position with respect to that of the primary vertex, where PDL is the *proper decay length*. The negative tail of the pull distribution of the J/ψ vertex position with respect to that of the primary vertex should be a Gaussian with a sigma of unity if uncertainties assigned to the vertex coordinates are correct. We ignore the positive side of the pull distribution as that tends to be biased towards larger values due to J/ψ mesons from real B meson decays. For this study we exclude electrons

from J/ψ decays from the primary vertex. The resulting pull distribution was fitted using a double Gaussian: the narrow Gaussian with width $\sigma_{narrow} = 0.97 \pm 0.12$ comprises 66% of the events, and the wide Gaussian with width $\sigma_{wide} = 1.83 \pm 0.30$ comprises 34%.

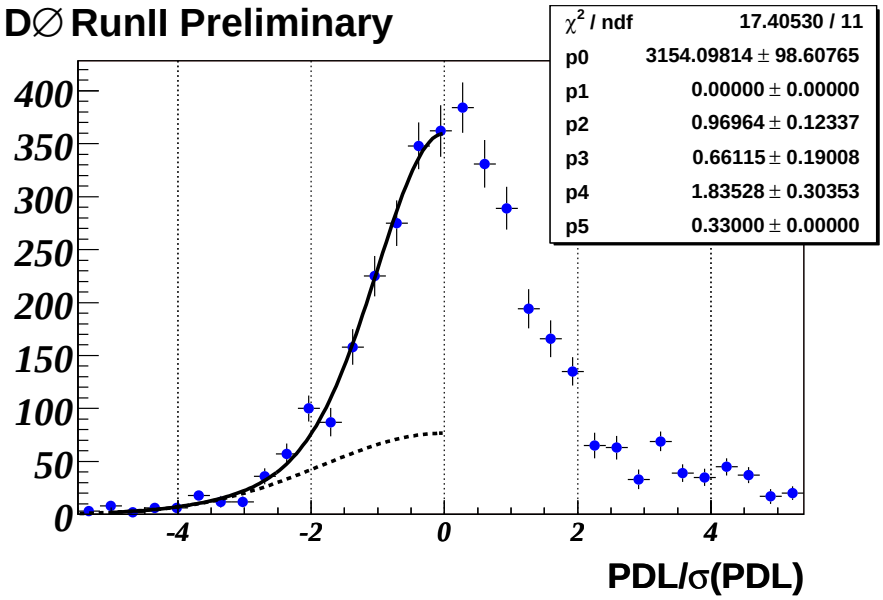

FIG. 14: Pull of J/ψ vertex distribution with respect to the Primary Vertex. We fit a double gaussian to the distribution with the relative fraction as a fit parameter. Parameter p1 is the mean of the two gaussians, fixed at 0.0. Parameter p5 is the binwidth which is fixed.

The total tagged data sample was used to determine the parameters from a lifetime fit to the background and signal region: $\mathcal{F}_{peak\_bkg} = 0.10 \pm 0.02$, $\sigma_{peak\_bkg} = 0.011 \pm 0.001$ μm, $\mathcal{F}_0 = 0.379 \pm 0.022$, $s_{bkg} = 2.027 \pm 0.003$, $c\tau_{bkg} = 645 \pm 18$ μm, $\mathcal{F}_{peak\_sig} = 0.11 \pm 0.03$, $\mathcal{F}_{tsens} = 0.50 \pm 0.13$, $\mathcal{F}_{osc} = 0.53 \pm 0.10$ and $c\tau_{B_s^0} = 444 \pm 29$ μm consistent with the world average value of 438 μm.

VIII. AMPLITUDE FIT METHOD

The amplitude fit method [16] is a technique that can be used to calculate an experimental Δm_s oscillation limit. The D_s^- sample is composed mostly of B_s^0 mesons with some contributions from B_u and B_d mesons. Different species of B mesons behave differently with respect to oscillations. Neutral B_d and B_s mesons do oscillate (with different frequencies), while charged B_u mesons do not. The possible contributions of b-baryons in the sample are expected to be small and so are neglected.

For a given type of B-hadron (i.e. d, u, s), the distribution of the visible proper decay length x is given by:

$$p_s^{nos}(x) = \frac{K}{c\tau_{B_s}} \exp(-\frac{Kx}{c\tau_{B_s}}) \cdot 0.5 \cdot (1 + \mathcal{A} \cdot \mathcal{D} \cos(\Delta m_s \cdot Kx/c)) \quad (25)$$

$$p_s^{osc}(x) = \frac{K}{c\tau_{B_s}} \exp(-\frac{Kx}{c\tau_{B_s}}) \cdot 0.5 \cdot (1 - \mathcal{A} \cdot \mathcal{D} \cos(\Delta m_s \cdot Kx/c)) \quad (26)$$

where τ is the lifetime of the B hadron, K is the K factor, which reflects the difference between the observable and true momenta of B-hadron, and $\mathcal{A}$ is a fit parameter. Different choices of Δm_s are input and the fitted value of $\mathcal{A}$ is returned. By plotting the fitted value of $\mathcal{A}$ as a function of the input value of Δm_s, one searches for a peak of $\mathcal{A}$=1 to obtain a measurement of Δm_s. If no peak is found, limits can easily be set using this method. The sensitivity of a measurement is determined by calculating the probability that $\mathcal{A}$=0 could fluctuate to $\mathcal{A}$=1. This occurs at the lowest value of Δm_s for which $1.645\ \sigma_{\Delta m_s} = 1$ for a 95% CL, where $\sigma_{\Delta m_s}$ is the uncertainty on the value of $\mathcal{A}$ at the point Δm_s. The limit is determined by calculating the probability that a fitted value of $\mathcal{A}$ could fluctuate to $\mathcal{A} = 1$. This occurs at the lowest value of Δm_s for which $\mathcal{A}_{\Delta m_s} + 1.645\sigma_{\Delta m_s} = 1$.

Figure 15 shows the dependence of the parameter $\mathcal{A}$ and its error on the Δm_s. A 95% confidence level limit on the oscillation frequency $\Delta m_s > 7.8$ ps^{-1} and sensitivity 8.2 ps^{-1} were obtained.

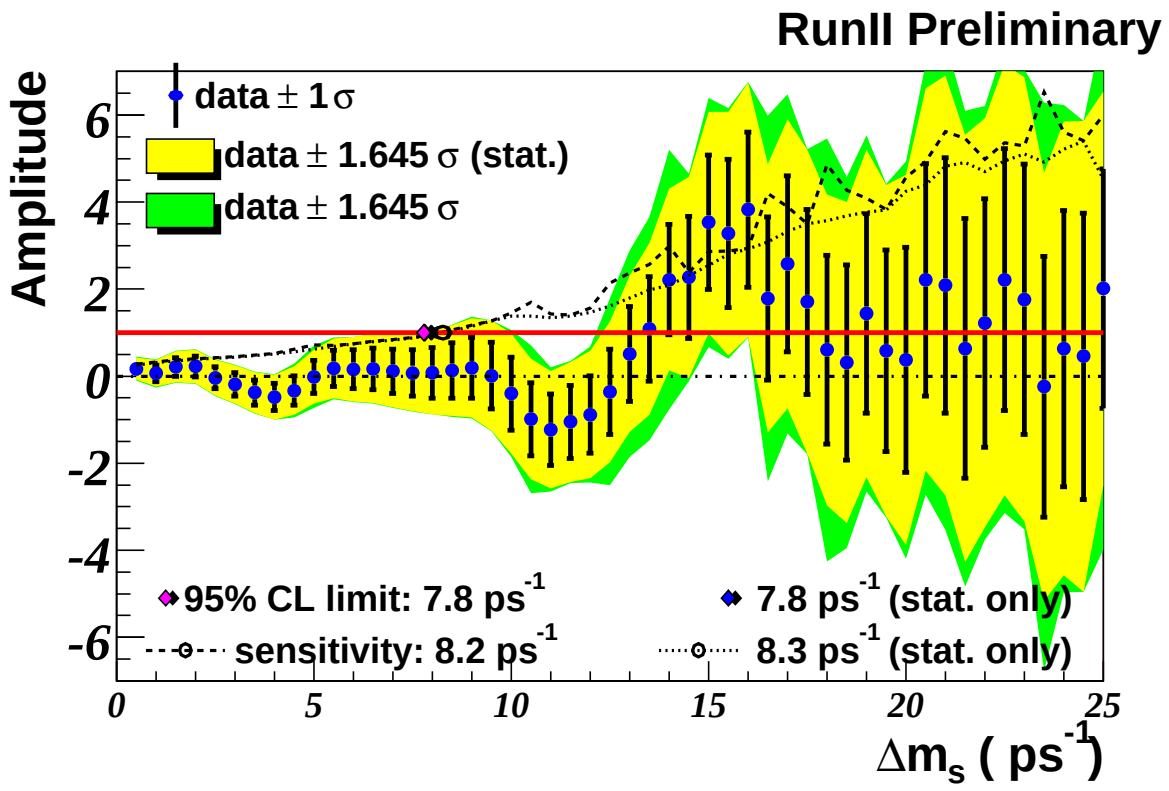

FIG. 15: B_s^0 oscillation amplitude with statistical and systematic errors. The dashed line shows the sensitivity including both statistical and systematic uncertainties.

IX. SYSTEMATIC UNCERTAINTIES

We perform a Δm_d amplitude scan to cross-check the dilution using the $B^0 \to D^{\pm}$ candidates. The resulting amplitude scan is shown in Figure 16. The amplitude at $\Delta M_d = 0.5$ ps^{-1} is in agreement with 1, that confirms a correctness of the dilution calibration. This cross-check also shows an ability of the method to detect an oscillation signal.

All studied contributions to the systematic uncertainty of the amplitude are listed in Table II. For each Δm_s step, the deviations of $\Delta\mathcal{A}$ and $\Delta\sigma_{\mathcal{A}}$ from the default values are given. The resulting systematic uncertainties were obtained using the formula from Ref. [16]

$$\sigma_{\mathcal{A}}^{sys} = \Delta\mathcal{A} + (1 - \mathcal{A})\frac{\Delta\sigma_{\mathcal{A}}}{\sigma_{\mathcal{A}}} \tag{27}$$

and were summed in quadrature. The effect of the systematic uncertainties is represented by the green (dark shaded) region in Fig. 15. Taking into account the systematic uncertainties, we obtained a 95% confidence level limit on the oscillation frequency $\Delta m_s > 7.8$ ps^{-1} and a expected limit of 8.2 ps^{-1}.

X. CONCLUSIONS

Using a sample of approximately 1000 $B_s^0 \to D_s^- e^+ \nu X$ decays, where $D_s^- \to \phi\pi^-$, $\phi \to K^+K^-$, in combination with an opposite-side flavor tagging algorithm and an unbinned fit, we performed a search for $B_s^0 - \bar{B}_s^0$ oscillations. We obtain a 95% confidence level limit on the oscillation frequency $\Delta m_s > 7.9 ps^{-1}$ and sisitivity 8.3 ps^{-1}.

Osc. frequency		1 ps^{-1}	3 ps^{-1}	5 ps^{-1}	7 ps^{-1}	9 ps^{-1}	11 ps^{-1}	13 ps^{-1}	15 ps^{-1}	17 ps^{-1}	19 ps^{-1}	21 ps^{-1}	23 ps^{-1}	25 ps^{-1}
$\mathcal{A}$		0.065	-0.187	-0.014	0.116	0.192	-1.229	0.514	3.533	2.579	1.439	2.087	1.766	2.011
Stat. uncertainty		0.188	0.268	0.378	0.507	0.695	0.820	1.091	1.546	2.021	2.288	2.933	3.102	2.753
$c\tau_{B_s}$	$\Delta\mathcal{A}$	-0.004	0.002	-0.001	-0.001	0.002	0.000	0.005	-0.008	-0.002	-0.023	-0.014	-0.012	-0.002
	$\Delta\sigma_{\mathcal{A}}$	-0.001	-0.001	-0.002	-0.002	-0.003	-0.003	-0.004	-0.008	-0.012	-0.011	-0.014	-0.009	-0.012
$\mathcal{F}_{peak\_sig}$	$\Delta\mathcal{A}$	0.001	0.002	-0.002	0.001	0.004	0.003	-0.004	-0.014	-0.009	-0.029	-0.036	-0.023	-0.004
	$\Delta\sigma_{\mathcal{A}}$	-0.001	-0.001	-0.002	-0.002	-0.003	-0.001	-0.003	-0.005	-0.007	-0.005	-0.005	0.007	0.012
Peaking bkg (bkg)	$\Delta\mathcal{A}$	0.002	0.002	-0.008	-0.005	0.000	0.006	-0.005	-0.030	0.006	0.003	0.029	0.027	0.021
	$\Delta\sigma_{\mathcal{A}}$	-0.002	-0.003	-0.004	-0.005	-0.006	-0.006	-0.009	-0.015	-0.019	-0.019	-0.027	-0.027	-0.032
F^0	$\Delta\mathcal{A}$	0.001	-0.001	-0.012	-0.007	-0.001	0.010	-0.009	-0.045	-0.008	-0.031	-0.041	-0.051	-0.029
	$\Delta\sigma_{\mathcal{A}}$	-0.003	-0.004	-0.005	-0.006	-0.009	-0.008	-0.013	-0.020	-0.024	-0.024	-0.035	-0.030	-0.028
$c\tau_{bkg}$	$\Delta\mathcal{A}$	0.006	0.001	-0.008	-0.003	-0.002	0.026	-0.013	-0.073	-0.035	-0.029	-0.074	-0.038	-0.044
	$\Delta\sigma_{\mathcal{A}}$	-0.002	-0.003	-0.005	-0.007	-0.010	-0.009	-0.015	-0.024	-0.026	-0.026	-0.040	-0.036	-0.019
σ_{peak_bkg}	$\Delta\mathcal{A}$	0.000	0.002	-0.003	-0.002	-0.002	0.020	-0.005	-0.062	-0.023	-0.019	-0.036	-0.031	-0.033
	$\Delta\sigma_{\mathcal{A}}$	-0.002	-0.002	-0.003	-0.004	-0.007	-0.007	-0.012	-0.021	-0.024	-0.025	-0.038	-0.038	-0.028
s_{bkg}	$\Delta\mathcal{A}$	0.001	0.001	-0.004	-0.002	-0.002	0.015	-0.007	-0.051	-0.013	-0.011	-0.022	-0.015	-0.017
(Scale fac. VPDL res.)	$\Delta\sigma_{\mathcal{A}}$	-0.002	-0.002	-0.003	-0.005	-0.007	-0.007	-0.011	-0.018	-0.023	-0.024	-0.036	-0.034	-0.029
$\mathcal{F}_{tsens}$	$\Delta\mathcal{A}$	-0.023	0.001	-0.005	-0.002	-0.003	0.017	-0.007	-0.069	-0.033	-0.016	-0.049	-0.072	-0.055
	$\Delta\sigma_{\mathcal{A}}$	-0.002	-0.002	-0.003	-0.005	-0.007	-0.007	-0.012	-0.020	-0.025	-0.029	-0.035	-0.030	-0.020
$\mathcal{F}_{osc}$	$\Delta\mathcal{A}$	-0.024	0.030	0.019	0.009	0.017	0.034	-0.003	-0.079	-0.040	-0.015	-0.028	-0.055	-0.039
	$\Delta\sigma_{\mathcal{A}}$	-0.002	-0.003	-0.003	-0.005	-0.007	-0.007	-0.012	-0.017	-0.024	-0.024	-0.035	-0.035	-0.028
N_{Ds}	$\Delta\mathcal{A}$	0.002	0.005	-0.011	-0.004	0.006	0.047	-0.009	-0.144	-0.068	-0.065	-0.104	-0.112	-0.061
	$\Delta\sigma_{\mathcal{A}}$	-0.005	-0.007	-0.009	-0.014	-0.020	-0.017	-0.029	-0.049	-0.061	-0.061	-0.088	-0.072	-0.049
K-factor variation (5%)	$\Delta\mathcal{A}$	-0.012	0.037	-0.169	0.052	-0.086	0.220	-0.883	-1.081	1.128	-0.983	-1.901	-0.889	-2.220
	$\Delta\sigma_{\mathcal{A}}$	-0.001	-0.002	-0.014	-0.013	-0.049	0.023	-0.134	-0.177	-0.138	-0.093	-0.397	-0.270	0.473
dilution	$\Delta\mathcal{A}$	0.000	0.002	-0.004	-0.002	-0.000	0.019	-0.007	-0.058	-0.019	-0.017	-0.031	-0.025	-0.023
	$\Delta\sigma_{\mathcal{A}}$	-0.002	-0.002	-0.003	-0.005	-0.007	-0.007	-0.012	-0.020	-0.024	-0.025	-0.037	-0.034	-0.027
$B_s^0 \to D_s D_s = 4.7\%$	$\Delta\mathcal{A}$	0.003	-0.004	-0.003	0.001	0.001	-0.017	0.004	0.043	0.032	0.020	0.033	0.040	0.038
	$\Delta\sigma_{\mathcal{A}}$	0.002	0.003	0.004	0.006	0.008	0.010	0.013	0.018	0.026	0.029	0.040	0.044	0.038
$B_s^0 \to D_s e\nu X = 5.5\%$	$\Delta\mathcal{A}$	-0.001	-0.004	-0.003	0.001	0.000	-0.014	0.003	0.038	0.028	0.021	0.029	0.026	0.028
	$\Delta\sigma_{\mathcal{A}}$	0.002	0.003	0.004	0.005	0.008	0.009	0.012	0.017	0.024	0.027	0.037	0.041	0.036
$p_T^{\mu\text{tag}} > 6$ (Compo.)	$\Delta\mathcal{A}$	0.003	-0.012	-0.010	-0.011	-0.018	0.007	0.003	-0.026	0.010	0.043	0.025	0.002	-0.009
	$\Delta\sigma_{\mathcal{A}}$	0.003	0.005	0.007	0.007	0.008	0.004	0.005	0.004	0.012	0.008	0.002	-0.014	-0.015
sf	$\Delta\mathcal{A}$	0.002	-0.002	-0.000	-0.000	0.000	-0.023	0.034	0.173	0.123	0.078	0.108	0.010	-0.007
(Sig. scale fac. VPDL res.)	$\Delta\sigma_{\mathcal{A}}$	0.000	0.002	0.004	0.008	0.013	0.018	0.030	0.044	0.081	0.104	0.140	0.133	0.121
Fraction (fit error)	$\Delta\mathcal{A}$	-0.005	0.011	-0.002	-0.031	-0.024	0.101	-0.114	-0.559	-0.519	-0.345	-0.433	-0.223	-0.161
(Sig. Pull Dist.)	$\Delta\sigma_{\mathcal{A}}$	-0.002	-0.008	-0.018	-0.033	-0.055	-0.076	-0.119	-0.184	-0.292	-0.367	-0.488	-0.463	-0.386
Total syst.	σ_{tot}^{sys}	0.065	0.056	0.214	0.057	0.149	0.286	0.944	0.801	1.238	0.972	1.759	0.836	2.397
Total	σ_{tot}	0.199	0.273	0.434	0.510	0.711	0.868	1.443	1.742	2.370	2.486	3.420	3.213	3.650

TABLE II: Systematic uncertainties on the amplitude. The shifts of both the measured amplitude, $\Delta\mathcal{A}$, and its statistical uncertainty, $\Delta\sigma$, are listed

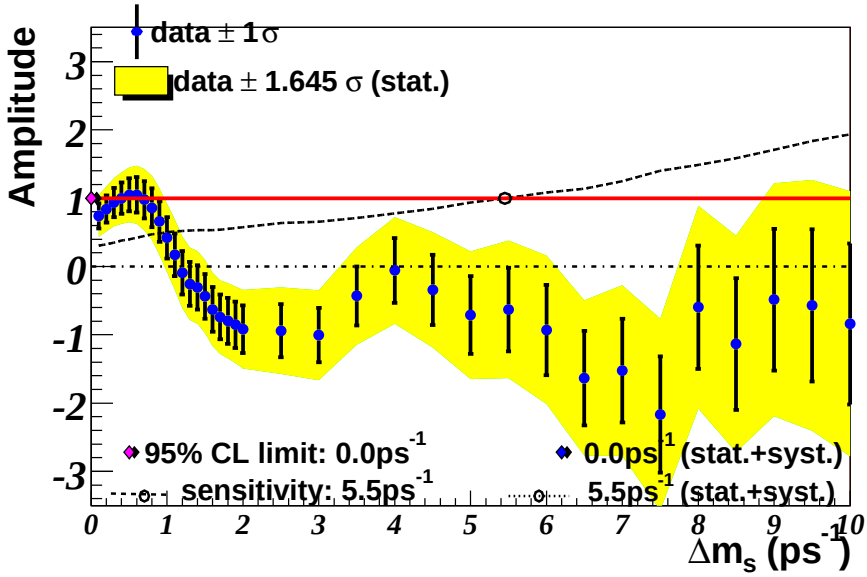

FIG. 16: $B_d - \bar{B}_d$ oscillation amplitude.

Acknowledgments

We thank the staffs at Fermilab and collaborating institutions, and acknowledge support from the DOE and NSF (USA); CEA and CNRS/IN2P3 (France); FASI, Rosatom and RFBR (Russia); CAPES, CNPq, FAPERJ, FAPESP and FUNDUNESP (Brazil); DAE and DST (India); Colciencias (Colombia); CONACyT (Mexico); KRF (Korea); CONICET and UBACyT (Argentina); FOM (The Netherlands); PPARC (United Kingdom); MSMT (Czech Republic); CRC Program, CFI, NSERC and WestGrid Project (Canada); BMBF and DFG (Germany); SFI (Ireland); Research Corporation, Alexander von Humboldt Foundation, and the Marie Curie Program.

[1] First Direct Two-Sided Bound on the Bs0 Oscillation Frequency, hep-ex/0603029; Submitted to Phys. Rev. Lett. *D0 Note 5045*, A Study of Mixing in the Bs System Using the Bs to DsMuX, Ds to PhiPi Decay Mode, Opposite-Side Flavor Tagging and Unbinned Fit, M.S.Anzelc, C.Ay, G.Borissov, S.Burdin, H.Evans, R.Jesik, T.Moulik, A.Nomerotski, Ph.Lewis, D.Strom, W.Taylor, D.Tsybychev, R. Van Kooten
[2] Measurement of the Bs-Bsbar Oscillation Frequency, CDF Collaboration, hep-ex/0606027,Submitted to Phys. Rev. Lett.
[3] CKM Fitter Group, *http://www.slac.stanford.edu/xorg/ckmfitter/ckm_welcome.html.*
[4] UTfit Collaboration, M. Bona *et al.*, J. High Energy Phys. **07**(2005) 028.
[5] V. Abazov *et al.* [DØ Collaboration] *The Upgraded DØ Detector*, submitted to Nucl. Instrum. Methods Phys. Res. A., arXiv:hep-physics/0507191, Fermilab-Pub-05/341-E.
[6] V. M. Abazov *et al.*, Nucl. Instrum. Meth. A **552**, 372 (2005).
[7] Central Preshower validation and Soft Electron Identification, Phil Baringer, Don Coppage, Tania Moulik, DØ Note 4920, Sep 19 2005.
[8] S. Catani, Yu.L. Dokshitzer, M. Olsson, G. Turnock, B.R. Webber, Phys.Lett. **B269** (1991) 432.
[9] T. Sjöstrand *et al.*, hep-ph/0108264.
[10] DELPHI Collab., *b-tagging in DELPHI at LEP*, Eur. Phys. J. **C32** (2004), 185-208.
[11] G. Borisov, Nucl. Instrum. Meth. A **417**, 384 (1998).
[12] The DØ Collaboration, *DØ Note 5029*, "B_d Mixing Measurement using Opposite-side Flavor Tagging".
[13] S. Eidelman *et al.*, Phys. Lett. **B592**, 1 (2004).
[14] F. James, *MINUIT - Function Minimization and Error Analysis*, CERN Program Library Long Writeup D506, 1998.
[15] D.J. Lange, Nucl. Instrum. Meth. A **462**, 152 (2001); for details see *http://www.slac.stanford.edu/~ lange/EvtGen.*
[16] H.G. Moser, A. Roussarie, Nucl.Instrum.Meth.A **384**, 491 (1997).